Interlayer hybridization in a van der Waals quantum spin-Hall insulator/superconductor heterostructure

Cite as: AIP Advances 13, 035115 (2023); doi: 10.1063/5.0130393
Submitted: 30 November 2022 • Accepted: 16 February 2023 •
Published Online: 8 March 2023

Fabio Bussolotti,[1,a] Hiroyo Kawai,[2] Ivan Verzhbitskiy,[1] Wei Tao,[3] Duc-Quan Ho,[3] Anirban Das,[4] Junxiang Jia,[3] Shantanu Mukherjee,[4] Bent Weber,[3,a] and Kuan Eng Johnson Goh[1,3,5,a]

AFFILIATIONS

[1] Institute of Materials Research and Engineering, Agency for Science Technology and Research (A∗STAR), 2 Fusionopolis Way, #08-03 Innovis, Singapore 138634, Republic of Singapore
[2] Institute of High Performance Computing, Agency for Science, Technology and Research, 1 Fusionopolis Way, #16-16 Connexis, Singapore 138632, Republic of Singapore
[3] Division of Physics and Applied Physics, School of Physical and Mathematical Sciences, Nanyang Technological University, 50 Nanyang Avenue, 639798, Singapore
[4] Department of Physics, Indian Institute of Technology Madras, Chennai 600036, India
[5] Department of Physics, National University of Singapore, 2 Science Drive 3, Singapore 117551, Singapore

[a] **Authors to whom any correspondence should be addressed:** b.fabio@imre.a-star.edu.sg; b.weber@ntu.edu.sg; and kejgoh@yahoo.com

ABSTRACT

In this work, we present an angle-resolved photoemission spectroscopy study of a $1T'$-WTe_2 monolayer epitaxially grown on $NbSe_2$ substrates, a prototypical quantum spin Hall insulator (QSHI)/superconductor heterojunction. Angle-resolved photoemission spectroscopy data indicate the formation of electronic states in the bulk bandgap of WTe_2, which are absent in the nearly free-standing WTe_2 grown on the highly oriented pyrolytic graphite substrate, where an energy gap of ~100 meV is reported. The results are explained in terms of hybridization effects promoted by the QSHI–superconductor interaction at $WTe_2/NbSe_2$ interfaces, in line with recent scanning probe microscopy investigation and theoretical band structure calculations. Our findings highlight the important role of interlayer interaction on the electronic properties and ultimately on the engineering of topological properties of the QSHI/superconducting heterostructure.

I. INTRODUCTION

Owing to their layered structure, van der Waals materials offer a unique platform to explore new quantum states of matter. Held together only by weak van der Waals forces in the bulk, individual atomically thin monolayers (MLs) often demonstrate properties uncommon to their bulk counterparts. This is well exemplified by a ML of $1T'$-WTe_2, which is a two-dimensional (2D) quantum spin Hall insulator (QSHI),[1] a topologically nontrivial quantum material characterized by helical edge states protected by time-reversal symmetry and the bulk (as opposed to the edge) bandgap opening due to the strong spin–orbit coupling.[1,2] Remarkably, inducing superconductivity in the helical edge states of QSHI has been theoretically predicted[1] to result in a topological superconductor, a highly sought-after state of matter[3] and a potential host for elusive Majorana fermions.[4,5] In this context, heterostructures of a QSHI with an *s*-wave superconductor (SC) offers a practical approach to engineering a topological superconducting state from various QSHI/SC combinations.[6–8] Among these, van der Waals heterostructures stand out as material systems with an atomically sharp, transparent interface that preserves the structural integrity of 2D constituents.[9] However, surface reconstruction,[10,11] electric fields

induced by charge transfer, as well as proximity effects may strongly alter their electronic band structure.[12] Recent scanning tunneling spectroscopy (STS) studies of van der Waals QSHI/SC heterostructure, $WTe_2/NbSe_2$, showed a clear signature of superconducting bulk and edge states,[7,8] suggesting that interlayer coupling and hybridization are strong across the van der Waals interface and are a promising candidate for the engineering of stable induced superconductivity at large pairing strength. Indeed, for both nanofabricated[7] and MBE grown samples,[8] STS indicates the formation of a residual 2D density in the nominally insulating 2D QSH bulk of $WTe_2/NbSe_2$ heterostructures.

Here, we present a detailed measurement of the electronic band structure of the $WTe_2/NbSe_2$ heterostructure by angle-resolved photoemission spectroscopy (ARPES) for the first time to gain further insight into interface coupling. New electronic states are observed in the bulk bandgap of ML WTe_2 that are otherwise absent in the nearly free-standing WTe_2 grown on the highly oriented pyrolytic graphite (HOPG) substrate. Theoretical analyses support the above observation, assigning the new states to the interlayer hybridization at the QSHI/SC interface that results in the formation of metallic states in the nominally gapped WTe_2.

II. RESULTS AND DISCUSSION

We performed ARPES measurements on a $1T'$-WTe_2 grown on a $NbSe_2$ ($WTe_2/NbSe_2$ in the following) and HOPG substrate (WTe_2/HOPG) by molecular beam epitaxy. The details of the sample preparation procedure and photoemission spectroscopy equipment are described in Sec. S1 (Fig. S1) and Sec. S2 of the supplementary material, respectively, identical to what was reported in Ref. 8. On both substrates, a coverage of 0.7 ML was achieved, as indicated by the Scanning Tunneling Microscopy (STM) characterization after sample preparation [Figs. S1(a) and S1(b) of the supplementary material].

Figures 1(a) and 1(b) show the schematic of the Surface Brillouin Zone (SBZ) of (a) $NbSe_2$ and (b) $WTe_2/NbSe_2$. The $NbSe_2$ and WTe_2 SBZ were reconstructed from the corresponding lattice constant values as extracted by the Scanning Tunneling Microscopy (STM) image analysis of the samples prepared under the same conditions[8] (see also Fig. S2 of the supplementary material), i.e., a_{NbSe2} = 3.4 Å, a_{WTe2} = 3.5 Å, and b_{WTe2} = 6.2 Å. The epitaxial growth condition results in the b_{WTe2} direction aligned along the $NbSe_2$ sublattices, i.e., the ΓY direction of $1T'$-WTe_2-SBZ parallel to the Γ*K* direction of the $NbSe_2$-SBZ (Fig. S2 of the supplementary material). However, due to the symmetry mismatch between the twofold rotational symmetry of the $1T'$-WTe_2 ML rectangular unit cell and the threefold symmetry of the $NbSe_2$ substrate, three energetically equivalent domains rotated by 120° [indicated as *D*1, *D*2, and *D*3 in Fig. 1(b)] exist.

Figure 1(c) reports the Fermi surface of the $NbSe_2$ crystal as obtained by ARPES via momentum-resolved, constant-energy intensity mapping around E_B = 0 eV (±10 meV) measured at 11 K. At low temperatures, the Fermi surface contour is enhanced due to reduced energy thermal broadening.[13] A hexagonal-like intensity pattern is observed reflecting the structure of the $NbSe_2$ SBZ in Fig. 1(a) with clearly distinguishable Γ*K* and ΓM directions [Fig. 1(c)]. Upon WTe_2 ML deposition on $NbSe_2$ a hexagonal-like Fermi surface is also observed [Fig. 1(d)], in apparent contrast with the rectangular symmetry of the WTe_2 ML-SBZ. The constant–energy map in Fig. 1(d) originates from the superimposition of the rectangular Fermi surfaces [Fig. 1(b)] of the 120°-rotated WTe_2 ML single-crystal domains (~20 nm lateral size, see Fig. S1 of the supplementary material) under the macroscopic area probed by ARPES (beam spot size ~0.8 mm, see experimental details in Sec. S2 of the supplementary material). A similar Fermi surface contour was reported previously in the ARPES study of WTe_2 ML epitaxially grown on a threefold symmetry graphene substrate.[14]

The in-plane multidomain orientation may, in principle, affect the band structure measurements of WTe_2 on $NbSe_2$, leading to the superimposition of the band dispersions along both the high-symmetry and non-high-symmetry directions of the SBZ [Fig. 1(b)]. In previous ARPES investigations of the 2D and 3D layered materials with similar in-plane multidomain structure, only band dispersions along the high-symmetry directions were detected.[15–17] The results were attributed to the higher density of states (DOS) along the high-symmetry directions with respect to other regions of the SBZ, resulting in the enhancement of the corresponding ARPES signal.[15–17] To minimize such superimposition effects, the band dispersion of WTe_2 on $NbSe_2$ was measured along the ΓY direction of the *D*1 domain, i.e., the $\Gamma Y^{(1)}$ [Fig. 1(b)] of WTe_2 parallel to the Γ*K* of the $NbSe_2$ surface [Fig. 1(a)], where only partial superimposition with no high-symmetry directions of equivalent rotated domains *D*2 and *D*3 is present [Fig. 1(b)]. The as-obtained electronic band structure for $NbSe_2$ and $WTe_2/NbSe_2$ at 11 K is plotted in Figs. 1(e) and 1(f). The raw Energy Distribution Curves (EDC) at different $k_{//}$ were normalized to the intensity of highest point within the plotted energy range, and the as obtained data are plotted in log scale to better capture the low intensity spectral features near the Fermi level (E_F).

ARPES data of WTe_2/HOPG at 11 K [Fig. 1(g), log-scale ARPES intensity plot] are also included for comparison purposes, where the full in-plane random orientation of WTe_2 domains and the corresponding SBZs led to the observed circular-like pattern in the constant energy ARPES intensity map [Fig. 1(h)].

Despite the WTe_2/HOPG multi-domain nature, a clear band structure is detectable. The experimental data are well described by the superimposition of the DFT calculated ΓX (dotted dark blue line) and ΓY (purple dashed line) band dispersion of a free-standing WTe_2 ML, their relative contribution to the measured ARPES intensity depending on the DOS as well as on the photoemission cross section and symmetry of the corresponding band wavefunctions.[14,17] The coexistence of a multidomain structure with measurable band dispersions is in line with previous ARPES study on 2D multidomain materials,[15–17] while the agreement between experimental data and theoretical band structure in Fig. 1(g) indicates weak interaction between the WTe_2 ML and HOPG, as reported in a previous ARPES study of the WTe_2/graphene interface.[14]

The $NbSe_2$ band structure signal [Fig. 1(e)] shows overall good agreement with the Density Functional Theory (DFT)-based prediction [white dotted lines in Fig. 1(e) (see Sec. S4 of the supplementary material for DFT calculation details) within the limit of first principles band structure calculations and ARPES signal intensity modulation reflecting the photon energy/polarization effect and emission direction.[13] We find that the $NbSe_2$ signal is strongly suppressed after WTe_2 layer deposition (thickness ~ 8 Å) due to the substrate coverage and the reduced photoelectron mean free path (~4 $Å^{-1}$)

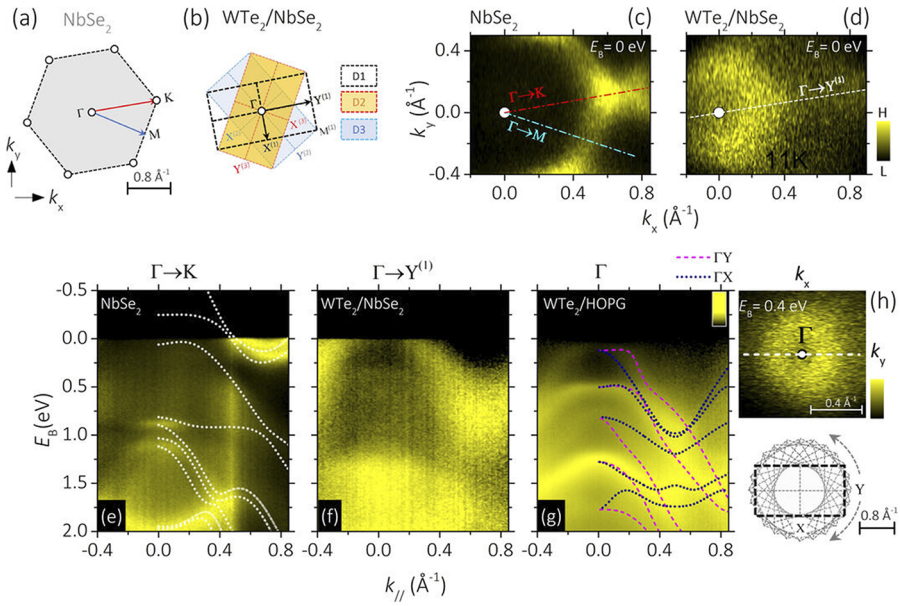

FIG. 1. [(a) and (b)] Schematic Surface Brillouin Zone (SBZ) of (a) $NbSe_2$ and (b) $WTe_2/NbSe_2$ with the corresponding three domain (D1, D2, and D3) orientations. k_x and k_y are the momentum directions in the laboratory reference system. [(c) and (d)] Constant energy ARPES intensity map (linear scale) of (c) $NbSe_2$ and (d) $WTe_2/NbSe_2$ in the (k_x, k_y) momentum space. Data were acquired ±10 meV around E_F (E_B = 0 eV) at 11 K. (e) ARPES intensity map (log scale) of the electronic band structure of $NbSe_2$ along the Γ*K* high symmetry direction as acquired at 11 K (see the main text for the details of data normalization). Theoretical calculations are overlaid as white dotted lines. (f) Electronic band structure of WTe_2(ML)/$NbSe_2$ along $\Gamma\Upsilon^{(1)}$ at 11 K. (g) Electronic band structure of WTe_2(ML)/HOPG at 11 K. Theoretical band structure along ΓX and ΓΥ for a free standing WTe_2 ML is plotted as (dark blue) dotted and (purple) dashed lines, respectively. (h) Constant energy ARPES intensity map (linear scale) of WTe_2/HOPG at 11 K. Data were acquired at ±10 meV around E_B = 0.4 eV. ARPES data in panel (g) were acquired along the scanning direction indicated by the dashed line.

in the probed kinetic energy range (10–20 eV).[18] In $WTe_2/NbSe_2$, a single, large dispersive band (width >1 eV) is instead visible [Fig. 1(f)] apparently crossing E_F along $\Gamma\Upsilon^{(1)}$ directions. By comparison with the ARPES data of WTe_2/HOPG [Fig. 1(g)], a good correspondence with the ΓΥ-low binding energy valence band (VB) of the nearly free-standing WTe_2 ML [Fig. 1(g)] can be found once an energy shift toward E_F is considered. Noteworthy is the very weak signal detected from the ΓX band at ~ 1 eV with respect to the HOPG case, in line with the reduced in-plane azimuthal disorder of the WTe_2 ML on $NbSe_2$ [Fig. 1(b)].

To clarify the above experimental findings, the electronic structure near E_F of $WTe_2/NbSe_2$ and WTe_2/HOPG was investigated in greater detail. Figure 2 reports the ARPES band mapping of [(a) and (b)] WTe_2/HOPG and [(f) and (g)] $WTe_2/NbSe_2$ as measured at [(a) and (f)] 297 K and [(b) and (g)] 11 K, respectively. The data were obtained by dividing the original ARPES signal for an energy resolution-convoluted Fermi–Dirac (FD) distribution at the measurement temperature to remove the intensity cut-off at E_F and highlight the hitherto-hidden valence band (VB) and conduction band (CB) features near E_F.[19]

The ARPES data of WTe_2/HOPG exhibit a clear intensity drop in the absence of quasiparticle peak structure above the VB maximum at Γ point [E_B = 0.1 eV, see energy distribution curve (EDCs) in Fig. 2(c)] up to E_B ~ 0.0 eV, where the photoemission signal from the occupied and/or thermally populated CB states near E_F are detected. The result agrees well with the band structure calculation [dotted lines in Figs. 2(a) and 2(b)] of free-standing WTe_2 ML predicting an energy gap along the ΓΥ direction. From the analysis of ARPES momentum energy distribution curves [MDCs, see Figs. 2(d) and 2(e)] (see Sec. S5 of the supplementary material), an energy gap value of E_{gap} = 0.10 ± 0.04 eV is estimated, which agrees well with the previously reported values for exfoliated and deposited WTe_2 ML.[20]

The ARPES band mapping of $WTe_2/NbSe_2$ [Figs. 2(f) and 2(g)] shows good agreement with the calculated ΓΥ VB of the free-standing WTe_2 ML [dotted lines in Figs. 2(f) and 2(g)] with a shift of 0.1 eV toward E_F with respect to the HOPG case [see EDC in Fig. 2(h)]. However, no clear ARPES intensity reduction or lack of quasiparticle peak is observed above the VB maximum located at E_B = 0 eV as confirmed by the MDC analysis at 297 and 11 K [Figs. 2(i) and 2(j)]. Remarkably, ARPES data for the $WTe_2/NbSe_2$ interface indicate a higher density of states in the bulk energy gap when compared to the free-standing ML case, represented by WTe_2 on HOPG. These new states may originate from the layer–substrate electronic hybridization effects in the $WTe_2/NbSe_2$ heterostructure.

In support of these findings, tight-binding band structure calculations were conducted for the bulk states of a free-standing WTe_2 ML [Fig. 2(k)] and $WTe_2/NbSe_2$ heterostructure [Fig. 2(l)] (see Sec. S6 of the supplementary material for calculation details). For a clear comparison with the experiment, the binding energy scale of theoretical curves was shifted to match the experimental VB position at the Γ point.

In comparison to free-standing WTe_2 ML [Fig. 2(k)], tight binding calculations for $WTe_2/NbSe_2$ [Fig. 2(l)] clearly shows the VB and CB states "smearing out" in the original bulk energy gap due

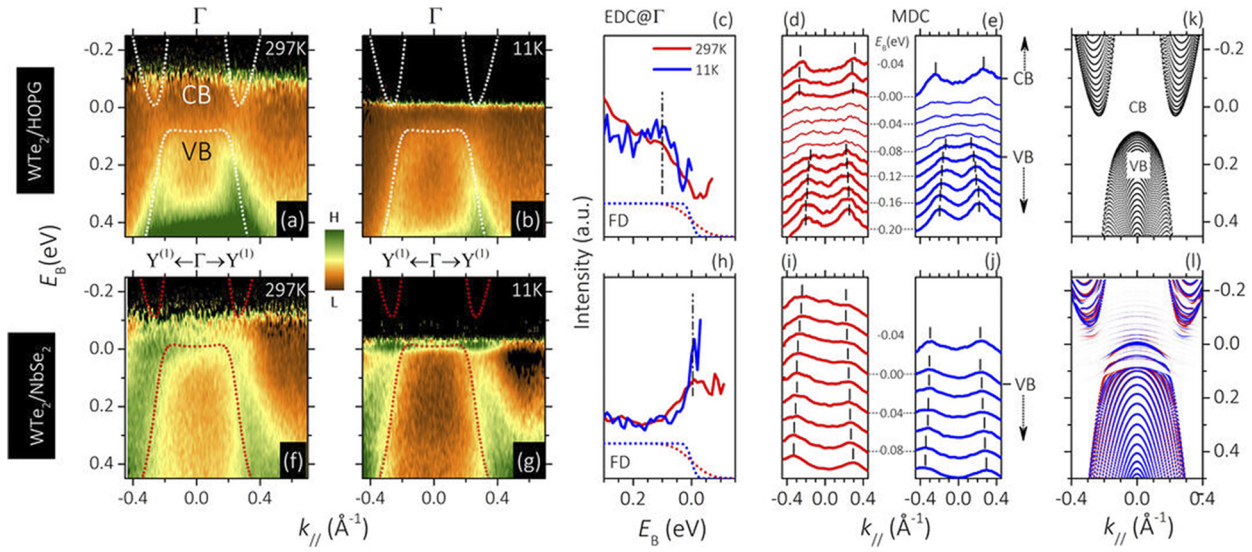

FIG. 2. [(a) and (b)] ARPES band mapping of WTe_2 (ML)/HOPG at (a) 297 K and (b) 11 K. Original ARPES data were divided by the energy-resolution convoluted Fermi–Dirac (FD) function at the indicated measurement temperatures to remove the cut-off near E_F. DFT-calculated valence band (VB) and conduction band (CB) structure along the ΓΥ symmetry directions are overlaid as dotted lines. Theoretical data were aligned at the experimental binding energy position of the VB at the Γ point. CB positions were adjusted to match the experimental energy gap values (see discussion in the text). (c) Energy distribution curves (EDC) at the Γ point (±0.01 $Å^{-1}$ integrated) of WTe_2 (ML)/HOPG at 297 and 11 K. Energy convoluted FD functions at the measured temperature are included as dotted lines. [(d) and (e)] WTe_2 (ML)/HOPG Momentum distribution curves (MDCs) across E_F at (d) 297 K and (e) 11 K. Quasiparticle peak momentum position is shown by the vertical bar. Thick and thin curve shows VB, CB, and energy gap binding energy region, respectively. [(f) and (g)] Same as in panels (a) and (b) for WTe_2 (ML)/$NbSe_2$ along the ΓΥ direction. (h) Same as in panel (c) for WTe_2 (ML)/$NbSe_2$. [(i) and (j)] Same as in panels (d) and (e) for WTe_2/$NbSe_2$ at (i) 297 K and (j) 11 K. [(k) and (l)] Tight binding (see the text for details) calculated ΓΥ band structure of a free-standing (k) WTe_2 ML and (l) WTe_2 ML on $NbSe_2$. The binding energy scale was shifted to align the calculated VB maximum to the experimental value of (k) WTe_2/HOPG and (l) WTe_2/$NbSe_2$.

to the layer–substrate interaction, thus, resulting a non-negligible density of states consistent with both our ARPES measurements and earlier scanning probe investigation.[8]

To better illustrate the above findings, we compared the calculated DOS of ML WTe_2 and WTe_2/$NbSe_2$ with the momentum-integrated ARPES signals, which reflect the energy levels' population in the examined heterostructures.[13] Figure 3 shows the tight-binding calculated DOS [Figs. 3(a) and 3(d)] with the WTe_2/HOPG and WTe_2/$NbSe_2$ momentum-integrated ARPES signal at 297 K [Figs. 3(b) and 3(e)] and 11 K [Figs. 3(c) and 3(f)] as obtained from experimental data presented in Figs. 2(a), 2(b), 2(f), and 2(g). ARPES data integration was limited to ±0.4 $Å^{-1}$ around the Γ point corresponding to the energy/momentum gap region.

At both 297 and 11 K, the integrated ARPES curves of WTe_2/HOPG monotonously drop above the VB maximum [vertical bar at $E_B \approx 0.1$ eV in Figs. 3(a)–3(c)], matching qualitatively well with the theoretical DOS of the freestanding WTe_2 ML [Fig. 3(a)], and thus highlighting the gapped nature of the bulk of WTe_2 ML on HOPG. For the WTe_2/$NbSe_2$ interface, however, the non-monotonous structure of VB edge and in-gap electronic states of theoretical DOS [marked by arrow in Fig. 3(d)] finds a good correspondence in the intensity peak of the momentum-integrated ARPES data at 297 K [Fig. 3(e)]. For 11 K integrated ARPES data of WTe_2/$NbSe_2$, a clear VB maximum is visible, yet the energy gap density is hidden by the signal divergence above E_F, which was introduced by the FD renormalization of the low temperature experimental data. Finally, the comparison with HOPG and $NbSe_2$ substrate data (see Fig. S7 for the corresponding ARPES raw data), also included in Figs. 3(b)–3(d), and 3(f), indicates their negligible contribution to the overall measured interface DOS even without considering the expected reduction of the substrate photoemission signal due to the WTe_2 deposition.[18] For the $NbSe_2$ case, the attenuated contribution of $NbSe_2$ (I_0') to the measured WTe_2/$NbSe_2$ ARPES signal around the Γ point can be estimated as $I_0' = (1 - C)I_0 + CI_0e^{-\frac{d}{\lambda}}$, where C is the WTe_2 coverage (expressed in ML), d is the WTe_2 thickness (~8 Å according to Ref. 8), and λ is the electron mean free path at the measured kinetic energy of photoelectrons (~4 Å).[18] For $C = 0.7$ ML (see Sec. S1 of the supplementary material), one has $I_0' = (1 - 0.7)I_0 + 0.7I_0e^{-\frac{8}{4}} = 0.39I_0$. According to the above calculations, the $NbSe_2$ substrate contributes only to ~30% of the total WTe_2/$NbSe_2$ ARPES signal around the Γ point [see Figs. 3(e) and 3(f)]. In this context, the $NbSe_2$ substrate has a reduced impact on the DOS measured in the energy gap of the WTe_2 on $NbSe_2$ as well on the large difference in the gap DOS between the WTe_2/$NbSe_2$ and WTe_2/HOPG system.

In principle, the observed ARPES signal in the energy gap region could also be associated with a larger energy broadening of the VB EDCs of WTe_2/$NbSe_2$, reflecting a poorer structural quality (i.e., defects, surface adsorbates, etc.) of the WTe_2 layer grown on the $NbSe_2$ substrate when compared to the growth on HOPG.[21,22] Due to energy broadening, introduced by the defect-mediated

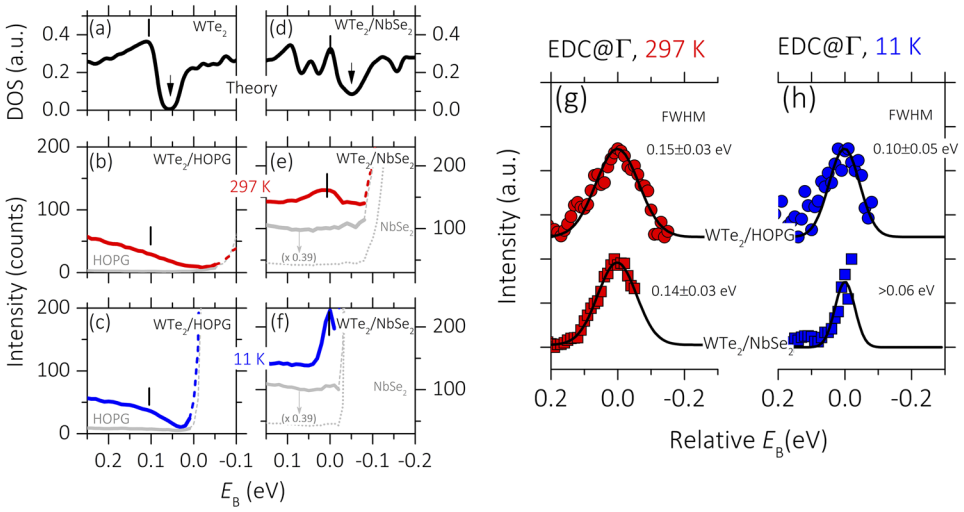

FIG. 3. (a) Tight-binding calculated DOS for the free-standing WTe_2 ML. [(b) and (c)] Integrated ARPES signal (±0.4 $Å^{-1}$ around Γ point) as obtained at (b) 297 K and (c) 11 K from the corresponding ARPES data in Fig. 2. Integrated ARPES data from the bare HOPG substrate are also included for comparison purposes. All the ARPES intensity data are renormalized by data integration time. The dashed line indicated the divergence of the experimental data following the renormalization process by FD function above E_F. (d) Same as in panel (a) for the $WTe_2/NbSe_2$ interface. [(e) and (f)] Same as in panels (b) and (c) for the $WTe_2/NbSe_2$ interface and $NbSe_2$ bare substrate. Dotted lines indicate the rescaled (×0.39) $NbSe_2$ bare substrate signal, according to its attenuation produced by WTe_2 deposition (see the main text for details). [(g) and (h)] Experimental EDCs around the Γ point at 297 K (g) and 11 K (h) for WTe_2/HOPG (upper curves) and $WTe_2/NbSe_2$ (lower curves) with the corresponding Gaussian peak fitting and as-extracted peak full width at half maximum (FWHM). Experimental data are the same as those presented in panels (c) and (h) of Fig. 2 after secondary electron background subtraction and normalization with respect to the high intensity point. Energy scale was aligned at the energy of the peak maximum.

modification of electronic states distribution and/or photoelectron scattering, the low energy tail of photoemission peaks may extend up to tenths of meV away from the VB maximum position, thus leading to an apparent increase in the photoemission signal inside the bulk energy gap. In this context, the 297 K- and 11 K-EDCs at the Γ point of WTe_2/HOPG and $WTe_2/NbSe_2$ [Fig. 2] were analyzed by the least square method and its full width at half maximum peak width (FWHM) was determined by Gaussian peak fitting. The results are reported in Figs. 3(g) and 3(h), showing, at all measured temperatures, comparable FWHMs values for the different telluride films, i.e., ~ 0.15 eV at 297 K and ~0.1 eV at 11 K, attesting to the quality of our WTe_2 films on both substrates and confirming that the additional 2D DOS observed in the bulk arises from layer–substrate hybridization largely absent in the WTe_2/HOPG interface.

Finally, we briefly comment on the VB energy difference of the WTe_2/HOPG and $WTe_2/NbSe_2$ interface [Figs. 2(a)–2(d)]. In principle, the ~0.1 eV "*p*-type like" VB shift observed in the $WTe_2/NbSe_2$ can also be related to a higher defect density as recently reported in photoemission studies of 2D semiconducting materials.[21] However, this is less likely on the basis of the peak fitting analysis presented above, indicating a comparable quality between the two fabricated heterostructures. Alternatively, the results can also be determined by the layer–substrate hybridization process and related gap states formation, which may alter the E_F position within the energy gap of the WTe_2 on $NbSe_2$ with respect to the HOPG case. In that regard, we also note that a comparable *p*-type like energy shift (~50 meV) was reported in previous STS mapping of WTe_2/NbS_2 and WTe_2/HOPG bulk DOS (see Fig. S8) in line with the present ARPES observation. More detailed investigation on the energy level alignment mechanism at the interface is required and in progress for complete understanding of the above observation.

To conclude, we have demonstrated evidence of WTe_2 and $NbSe_2$ hybridization using ARPES, in excellent agreement with prior scanning probe investigation and theoretical calculations. Our results demonstrate the suitability of ARPES technique as a prime tool to investigate the electronic band structure of the QSHI/superconducting electronic structure, complementary to the recent scanning probe investigations results.[7,8]

III. CONCLUSION

In this work, we reported an ARPES investigation of the electronic properties of the $1T'$-$WTe_2/NbSe_2$ heterostructure, a prototypical QSHI/superconducting interface, produced by molecular beam epitaxy. The formation of electronic states in the original bandgap of $1T'$-WTe_2 ML is detected as confirmed by comparison with the ARPES study of the nearly free standing $1T'$-WTe_2 ML on graphite. The results are explained in terms of layer–substrate hybridization at the ML/substrate interfaces, resulting in the formation of metallic states in the nominally gapped WTe_2 ML. The present results show direct evidence of the perturbation of QSHI's electronic properties via substrate interaction and provides insight on the interaction between ML WTe_2 and $NbSe_2$ and its impact on the electronic band structure. We also demonstrated ARPES as a suitable tool for increasing our understanding of the QSHI/superconductor interface beyond the nanoscale-limited information provided by scanning probe-based investigations.

SUPPLEMENTARY MATERIAL

See the supplementary material for the details on the experimental setup, sample preparation, STM and STS data, and band structure calculations.

ACKNOWLEDGMENTS

This research was supported by the National Research Foundation (NRF) Singapore, under the Competitive Research Program "Toward On-Chip Topological Quantum Devices" (Grant No. NRF-CRP21-2018-0001) F.B., H.K., I.V., and K.E.J.G. acknowledge the funding support from the Agency for Science, Technology and Research (Grant No. 21709). B.W. acknowledges support from the Singapore Ministry of Education (MOE) Academic Research Fund Tier 3 Grant (No. MOE2018-T3-1-002) and acknowledges the Singapore National Research Foundation (NRF) Fellowship (Grant No. NRF-NRFF2017-11). H.K. acknowledges the A*STAR Computational Resource Center (A*CRC) for computational resources and support.

AUTHOR DECLARATIONS

Conflict of Interest

The authors have no conflicts to disclose.

Author Contributions

Fabio Bussolotti: Data curation (lead); Formal analysis (lead); Investigation (lead); Methodology (lead); Writing – original draft (lead); Writing – review & editing (lead). **Hiroyo Kawai**: Methodology (equal); Writing – review & editing (equal). **Ivan Verzhbitskiy**: Writing – review & editing (equal). **Wei Tao**: Writing – review & editing (equal). **Duc-Quan Ho**: Writing – review & editing (equal). **Anirban Das**: Writing – review & editing (equal). **Junxiang Jia**: Writing – review & editing (equal). **Shantanu Mukherjee**: Writing – review & editing (equal). **Bent Weber**: Conceptualization (equal); Writing – review & editing (equal). **Kuan Eng Johnson Goh**: Conceptualization (equal); Writing – review & editing (equal).

DATA AVAILABILITY

The data that support the findings of this study are available from the corresponding authors upon reasonable request.

REFERENCES

[1] M. S. Lodge, S. A. Yang, S. Mukherjee, and B. Weber, "Atomically thin quantum spin Hall insulators," Adv. Mater. **33**, 2008029 (2021).
[2] S. Murakami, "Quantum spin Hall effect and enhanced magnetic response by spin-orbit coupling," Phys. Rev. Lett. **97**, 236805 (2006).
[3] M. Sato and Y. Ando, "Topological superconductors: A review," Rep. Prog. Phys. **80**, 76501 (2017).
[4] L. Fu and C. L. Kane, "Superconducting proximity effect and Majorana fermions at the surface of a topological insulator," Phys. Rev. Lett. **100**, 096407 (2008).
[5] J. Alicea, "New directions in the pursuit of Majorana fermions in solid state systems," Rep. Prog. Phys. **75**, 076501 (2012).
[6] K. Flensberg, F. von Oppen, and A. Stern, "Engineered platforms for topological superconductivity and Majorana zero modes," Nat. Rev. Mater. **6**, 944 (2021).
[7] F. Lüpke, D. Waters, S. C. de la Barrera, M. Widom, D. G. Mandrus, J. Yan, R. M. Feenstra, and B. M. Hunt, "Proximity-induced superconducting gap in the quantum spin Hall edge state of monolayer WTe_2," Nat. Phys. **16**, 526 (2020).
[8] W. Tao, Z. J. Tong, A. Das, D.-Q. Ho, Y. Sato, M. Haze, J. Jia, Y. Que, F. Bussolotti, K. E. J. Goh, B. Wang, H. Lin, A. Bansil, S. Mukherjee, Y. Hasegawa, and B. Weber, "Multiband superconductivity in strongly hybridized $1T'$-WTe_2/$NbSe_2$ heterostructures," Phys. Rev. B **105**, 094512 (2022).
[9] A. K. Geim and I. V. Grigorieva, "Van der Waals heterostructures," Nature **499**, 419 (2013).
[10] J. Kang, J. Li, S.-S. Li, J.-B. Xia, and L.-W. Wang, "Electronic structural Moiré pattern effects on MoS_2/$MoSe_2$ 2D heterostructures," Nano Lett. **13**, 5485 (2013).
[11] S. S. Sunku, G. X. Ni, B. Y. Jiang, H. Yoo, A. Sternbach, A. S. McLeod, T. Stauber, L. Xiong, T. Taniguchi, and K. Watanabe, "Photonic crystals for nano-light in Moiré graphene superlattices," Science **362**, 1153 (2018).
[12] K. S. Novoselov, A. Mishchenko, A. Carvalho, and A. H. Castro Neto, "2D materials and van Der Waals heterostructures," Science **353**, aac9439 (2016).
[13] A. Damascelli, Z. Hussain, and Z.-X. Shen, "Angle-resolved photoemission studies of the cuprate superconductors," Rev. Mod. Phys. **75**, 473 (2003).
[14] S. Tang, C. Zhang, D. Wong, Z. Pedramrazi, H.-Z. Tsai, C. Jia, B. Moritz, M. Claassen, H. Ryu, S. Kahn, J. Jiang, H. Yan, M. Hashimoto, D. Lu, R. G. Moore, C.-C. Hwang, C. Hwang, Z. Hussain, Y. Chen, M. M. Ugeda, Z. Liu, X. Xie, T. P. Devereaux, M. F. Crommie, S.-K. Mo, and Z.-X. Shen, "Quantum spin Hall State in monolayer $1T'$-WTe_2," Nat. Phys. **13**, 683 (2017).
[15] D. N. Basov, M. M. Fogler, A. Lanzara, F. Wang, and Y. Zhang, "Colloquium: Graphene spectroscopy," Rev. Mod. Phys. **86**, 959 (2014).
[16] F. Bussolotti, H. Kawai, S. L. Wong, and K. E. J. Goh, "Protected hole valley states in single-layer MoS_2," Phys. Rev. B **99**, 045134 (2019).
[17] F. Bussolotti, J. Chai, M. Yang, H. Kawai, Z. Zhang, S. Wang, S. L. Wong, C. Manzano, Y. Huang, D. Chi, and K. E. J. Goh, "Electronic properties of atomically thin MoS_2 layers grown by physical vapour deposition: Band structure and energy level alignment at layer/substrate interfaces," RSC Adv. **8**, 7744 (2018).
[18] M. P. Seah and W. A. Dench, "Quantitative electron spectroscopy of surfaces: A standard data base for electron inelastic mean free paths in solids," Surf. Interface Anal. **1**, 2 (1979).
[19] K. Kuroda, T. Tomita, M.-T. Suzuki, C. Bareille, A. A. Nugroho, P. Goswami, M. Ochi, M. Ikhlas, M. Nakayama, S. Akebi, R. Noguchi, R. Ishii, N. Inami, K. Ono, H. Kumigashira, A. Varykhalov, T. Muro, T. Koretsune, R. Arita, S. Shin, T. Kondo, and S. Nakatsuji, "Evidence for magnetic weyl fermions in a correlated metal," Nat. Mater. **16**, 1090 (2017).
[20] Y. Maximenko, Y. Chang, G. Chen, M. R. Hirsbrunner, W. Swiech, T. L. Hughes, L. K. Wagner, and V. Madhavan, "Nanoscale studies of electric field effects on monolayer $1T'$-WTe_2," Npj Quantum Mater. **7**, 29 (2022).
[21] F. Bussolotti, J. Yang, H. Kawai, C. P. Y. Wong, and K. E. J. Goh, "Impact of S-vacancies on the charge injection barrier at the electrical contact with the MoS_2 monolayer," ACS Nano **15**, 2686 (2021).
[22] W. Chen, G. Khaliullin, and O. P. Sushkov, "Coulomb disorder effects on angle-resolved photoemission and nuclear quadrupole resonance spectra in cuprates," Phys. Rev. B **80**, 094519 (2009).